



Deformation Behaviors of Flat Rolled Wire in Twinning-Induced Plasticity Steel

Joong-Ki Hwang¹

Received: 29 April 2019 / Accepted: 7 July 2019 / Published online: 19 July 2019
© The Korean Institute of Metals and Materials 2019

Abstract

The influence of room temperature flat rolling on microstructure, mechanical properties, and shape change in twinning-induced plasticity (TWIP) steel wire has been investigated to understand the deformation behaviors of flat rolled wire in TWIP steel and to apply TWIP steels to flat rolled wire products. Numerical simulation, hardness test, and EBSD techniques were used to analyze the distribution of strain, mechanical properties, and microstructure of flat rolled TWIP steel wire. The shape of flat rolled TWIP steel wire was also evaluated and compared with plain carbon steels having low strain hardening rate. A very different behavior of hardness, strain, twinning, and KAM value was observed with area of flat rolled wire due to the different stress state and strain with area of wire. The center area had the maximum twin density, KAM value, effective strain, and hardness; whereas free surface area had the minimum values. The hardness inhomogeneity factor (HIF) along the horizontal direction was much higher in comparison with that of the vertical direction. The maximum HIF value occurred at the specific reduction in height, i.e., 27%. This means HIF value gradually increased and then decreased with reduction in height, which is inconsistent with the results of plain carbon steel and Cu wire. The lateral spread and width of contact area of flat rolled TWIP steel wire were lower than those of plain carbon steels, indicating that material properties such as strain hardening exponent are crucial parameters that influence the shape of flat rolled wire products.

Keywords Twinning-induced plasticity (TWIP) steel · Flat rolled wire · Strain inhomogeneity · Shape of wire · Strain hardening exponent

1 Introduction

Wire drawing is an essential metal forming process to produce wire rod products such as springs, fasteners, bearings, and cables in the wire, rod, and bar industries. Shape rolling process, e.g., wire rod rolling, is also widely used in the same industries to make specific cross-sectional long products. Shape rolling process is usually conducted under the hot working condition in order to increase the formability of workpiece and to reduce the required energy. Meanwhile, the use of cold rolling process for shaped long products can be gradually increased in place of wire drawing process since rolling process has several advantages over wire drawing process in the view of manufacturing process as follows [1–3]:

- (i) Surface preparations prior to rolling process are very simple and easy: only mechanical descaling is sufficient before rolling process. In contrast, chemical pickling and phosphate coating are strongly necessary before wire drawing process. It reduces the total manufacturing cost and keeps the environment clean. It should be noted that the government is gradually regulating the use of environmental pollutants.
- (ii) Rolling process reduces the possibility of breakage of wire during process because wire is not subjected to tensional stress during rolling process.
- (iii) Rolling process offers much higher reduction ratio per pass without fracture compared to wire drawing process, leading to increase the productivity.
- (iv) During wire drawing, drawing speed is restricted since temperature rise stemming from the frictional stress in wire-die interface makes the wire more brittle and eventually causes the wire to break by strain aging mechanism, leading to decrease the productivity. In

✉ Joong-Ki Hwang
jkhwang@tu.ac.kr

¹ School of Mechanical Engineering, Tongmyong University,
Busan 48520, Republic of Korea

general, the temperature rise of wire is proportional to the drawing speed during wire drawing process.

- (v) Rolling process allows us to reduce the wear of tools as compared to wire drawing process by changing the frictional mechanism from shearing to rolling. That is, only a small relative motion between roll and wire is applied during rolling process.

In addition, several metallurgists have applied commercial metals such as low carbon steels [4–7], high carbon steels [8, 9], TWIP steels [10, 11], magnesium alloys [12], titanium alloys [13, 14], and clad composites [15, 16] to shape rolling process since shape rolled metals metallurgically have a variety of advantages. The simplest way of wire rod shape rolling process is flat rolling, which deforms the round wire using flat rolls at room temperature [17]. As shown in Fig. 1, the wire with round cross section is deformed into a flat wire with round edge on both sides by flat rolls. Flat rolled wires are typically used as springs, piston segments, saw blades, guide rails, trolley cables, windshield wipers of car, and electronic parts [18]. The first issue for manufacturing flat rolled wire is the shape control since the round wire is not deformed in the condition of plane strain such as flat rolling of sheet and a lateral spread always occurs in free surface, which means the shape control of wire is not easy during flat rolling process. Consequently, several researchers have investigated on the lateral spread of flat rolled wire with process conditions such as reduction in height, initial wire size, lubricant, and rolling speed using empirical, analytical, and numerical methods [18–23]. They found that the lateral spread of flat rolled wire increased

with increasing reduction in height and it was not sensitive to the rolling speed. Second issue is the inhomogeneity of mechanical properties of wire with area originating from the applied stress state during flat rolling process. Accordingly, effective strain and hardness distributions of flat rolled wire were well reported, especially using finite element (FE) analysis [24–27]. Their investigations showed that deformation inhomogeneity was increased with decreasing reduction in height and increasing friction coefficient.

Recently, Hwang et al. [28, 29] suggested that TWIP steel is one of the breakthrough materials for high strength wire rod products since TWIP steels meet the demanding property requirements of wire rod application due to their excellent combination of high strength, extraordinary ductility [30–37], high resistance to hydrogen-delayed fracture [10, 38], and lower total production cost in comparison with the plain carbon steels that are commercially used for wire rod products. Therefore, flat rolled wire products manufactured by TWIP steel have many advantages compared to those by commercial plain carbon steels such as pearlitic, tempered martensitic, and ferritic steels. Meanwhile, flat rolled wire industries also require high strength materials to meet the recent market needs and to strengthen the market competitiveness.

During the last three decades, many researchers have studied about the effect of external process conditions on shape change and inhomogeneity of mechanical properties with area of flat rolled wire, but only a few works have been reported on the effect of material properties itself. Kazeminezhad and Karimi Taheri [19] showed that material properties did not affect the lateral spread and width of contact area of wire by

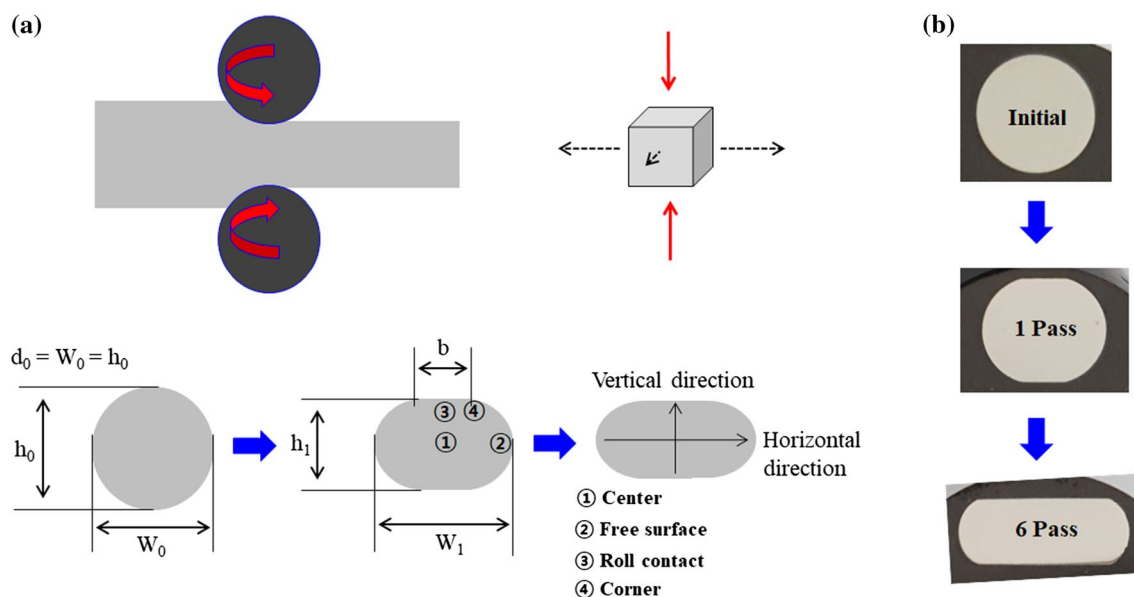


Fig. 1 **a** Schematic of cross-sectional shape and **b** measured cross-sectional shape of flat rolled TWIP steel wires

comparing high carbon steel and low carbon steel. In addition, most of the researchers have dealt with Cu wire and plain carbon steels, and no article has been found on the TWIP steels. It should be noted that the flat rolling behavior of TWIP steel wire can be different from that of Cu wire and plain carbon steel wire since TWIP steels have much higher strain hardening rate than Cu and plain carbon steels and they are deformed by different plastic deformation mechanism, i.e., deformation twinning [39]. That is, the final shape and inhomogeneity of mechanical properties with area of flat rolled TWIP steel wire can be different from those of plain carbon steels due to the higher strain hardening rate and twin deformation mechanism of TWIP steel.

Therefore, the present paper deals with the influence of flat rolling on microstructure, mechanical properties, and shape change in TWIP steel wire to understand the flat rolling behaviors of TWIP steel wire and to apply TWIP steels to flat rolled wire products such as spring and windshield wiper of car. Numerical simulation and hardness test were simultaneously conducted to analyze the distribution of strain and mechanical properties with area in flat rolled wire. And then electron backscatter diffraction (EBSD) techniques rationalized the mechanical properties of wire with area. Based on the results in TWIP steel, the shape change of flat rolled TWIP steel wire was compared with the plain carbon steels having low strain hardening rate, which might be helpful to understand the effect of material properties on flat rolling behaviors of wire.

2 Experimental Procedures

The TWIP steel used in the present study was fabricated by vacuum induction method under an Ar atmosphere and its analyzed chemical composition is listed in Table 1. The calculated stacking fault energy (SFE) of the present steel based on thermodynamics approach of Saeed-Akbari et al. [40] was estimated at 27.2 mJ/m² at room temperature. During the room temperature plastic deformation, deformation twinning and dislocation slip are expected to mainly occur in this steel, while ϵ -martensite should be suppressed.

Prior to hot rolling, the cast ingot of 125 mm in thickness was homogenized at 1200 °C for 3 h. And then the ingot was directly rolled to a plate of 20 mm in thickness using multi-pass rolling at temperature above 950 °C, followed by ambient cooling in order to simulate hot rod rolling process. The hot rolled plate was machined into several round bars with a diameter of 13 mm for flat rolling test.

Table 1 Analyzed chemical composition in weight percent and calculated SFE of the TWIP steel used in the present study

C	Mn	Al	Fe	SFE (mJ/m ²)
0.66	17.10	1.75	Bal.	27.2

Figure 1a depicts the schematic of flat rolling process and cross-sectional shape of workpiece during process. Flat rolling experiments were performed up to six pass by two rolls with the diameter of 400 mm, and rolling speed was set as 5 RPM to ignore the effect of temperature rise. The height of specimen was reduced by average 10% without lubricant. Reduction in height is calculated using Eq. (1).

$$R_h = \frac{h_0 - h_1}{h_0} \times 100 (\%) \quad (1)$$

where h_0 refers to the initial height of specimen and h_1 is the final height of specimen as shown in Fig. 1a. Since TWIP steels are strain-rate-sensitive materials, average strain rate during flat rolling was evaluated using the following equation, which is generally used for calculating the average strain rate during plate rolling.

$$\dot{\epsilon}_{ave} = \frac{v}{\sqrt{R_d}(h_0 - h_1)} \ln \frac{h_0}{h_1} \quad (2)$$

where v is the roll circumferential speed (105 mm s⁻¹). R_d means the deformed roll radius and was assumed to be the roll radius (200 mm) in this study. The calculated average strain rate per pass was between 0.69 and 0.92 and summarized in Table 2. The detailed processing parameters and cross-sectional shape of rolled wires are shown in Table 2 and Fig. 1b.

Round type tensile specimens (gauge diameter of 5 mm and length of 25 mm) were prepared along the rolling direction for uniaxial tensile tests. They were tested at an initial strain rate of 10⁻³ s⁻¹ using an Instron machine at room temperature. To evaluate the inhomogeneity of mechanical properties in flat rolled wire, Vickers hardness test was employed using 1 kg weight at each pass over the transverse cross-sectional plane perpendicular to the rolling axis.

The microstructure of flat rolled wire was examined by EBSD at four individual sites, i.e., center, free surface, roll contact surface, and corner areas, as shown in Fig. 1a. Specimens for EBSD measurement were carefully prepared by standard mechanical polishing down to 1 μ m using diamond pastes and colloidal silica slurry polishing. Field emission SEM equipped with a TSL EBSD system was used and it was operated at an acceleration voltage of 20 keV. EBSD maps with the observation area of 70 μ m \times 70 μ m or 140 μ m \times 140 μ m were acquired using the spatial step size of 0.1 μ m under the tilting angle of approximately 70° relative to normal incidence of electron beam. And then they were post-processed by the orientation imaging microscopy (OIM) commercial software. Microstructural characterizations were also performed on the cross section area of samples perpendicular to the rolling axis.

Table 2 Process parameters for six-pass flat rolling test in this experiment

No. of pass	Roll gap (mm)	Reduction in height per pass (%)	Total reduction in height (%)	Average strain rate (s ⁻¹)
1	11.63	10.0	10.0	0.69
2	10.50	9.4	18.5	0.70
3	9.40	10.4	27.0	0.78
4	8.45	10.5	34.6	0.83
5	7.50	10.6	41.5	0.88
6	6.75	10.5	47.7	0.92

3 Results and Discussion

3.1 Mechanical Properties

The tensile curve of hot rolled TWIP steel shows a typical characteristics of TWIP steel with carbon [41] as shown in Fig. 2. Yield strength, ultimate tensile strength, and total elongation were 395 MPa, 893 MPa, and 66.3%, respectively. This steel exhibited high strain hardening rate (Fig. 2b), serration, and small post-necking elongation (inset in Fig. 2a).

Figure 3a shows the measured average hardness with reduction in height. As expected, average hardness was increased with reduction in height. Hardness profiles along the horizontal direction and vertical direction are shown in Fig. 3b, c, respectively. The maximum hardness occurred at around center area, and surface area had minimum value. To evaluate the level of inhomogeneity, the hardness inhomogeneity factor (HIF) was defined as following equation:

$$HIF = \frac{H_{max} - H_{min}}{H_{average}} \quad (3)$$

where H_{max} , H_{min} , and $H_{average}$ are the hardness of maximum, minimum, and average, respectively. A larger HIF

implies a larger difference of hardness in the cross section of specimens. Figure 3d shows the HIF with reduction in height. Interestingly, HIF value gradually increased and then decreased with reduction in height, which means the maximum HIF value occurred at the specific reduction in height, i.e., 27%. This result is inconsistent with the results of Kazeminezhad and Karimi Taheri [25]. They reported that the deformation inhomogeneity had a simple trend with reduction in height using Cu wire with the diameter of 8 mm: deformation inhomogeneity was decreased with increasing reduction in height. It means that deformation inhomogeneity of flat rolled wire was dependent on the material properties, wire size, and other process conditions. Overall, it is worth noting that this result is very useful for industrial applications since one can produce flat rolled wires with more homogeneous mechanical properties by controlling the total reduction in height of wire. Meanwhile, the HIF values along the horizontal direction were much higher in comparison with those of the vertical direction. For instance, the maximum HIF value along the horizontal direction was about three times higher than that along the vertical direction.

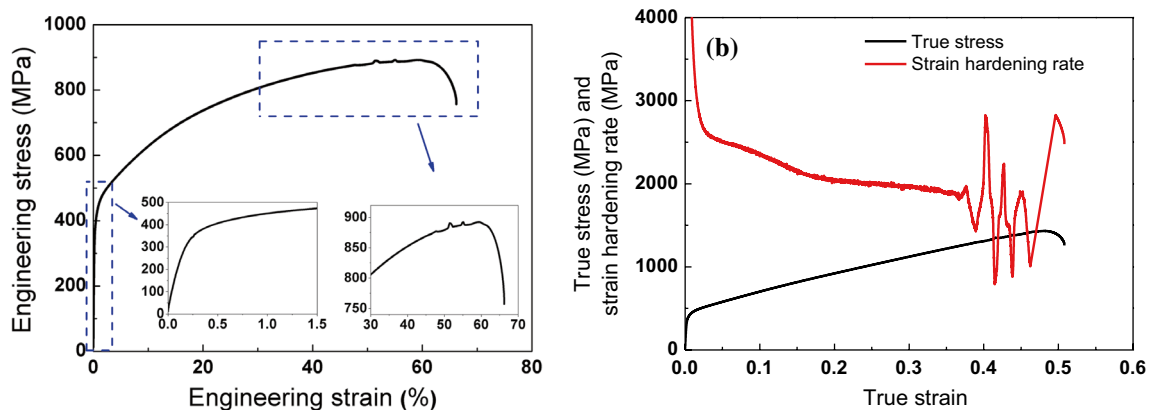


Fig. 2 a Engineering stress–strain curve and b true stress–strain curve and corresponding strain hardening rate curve of hot rolled TWIP steel

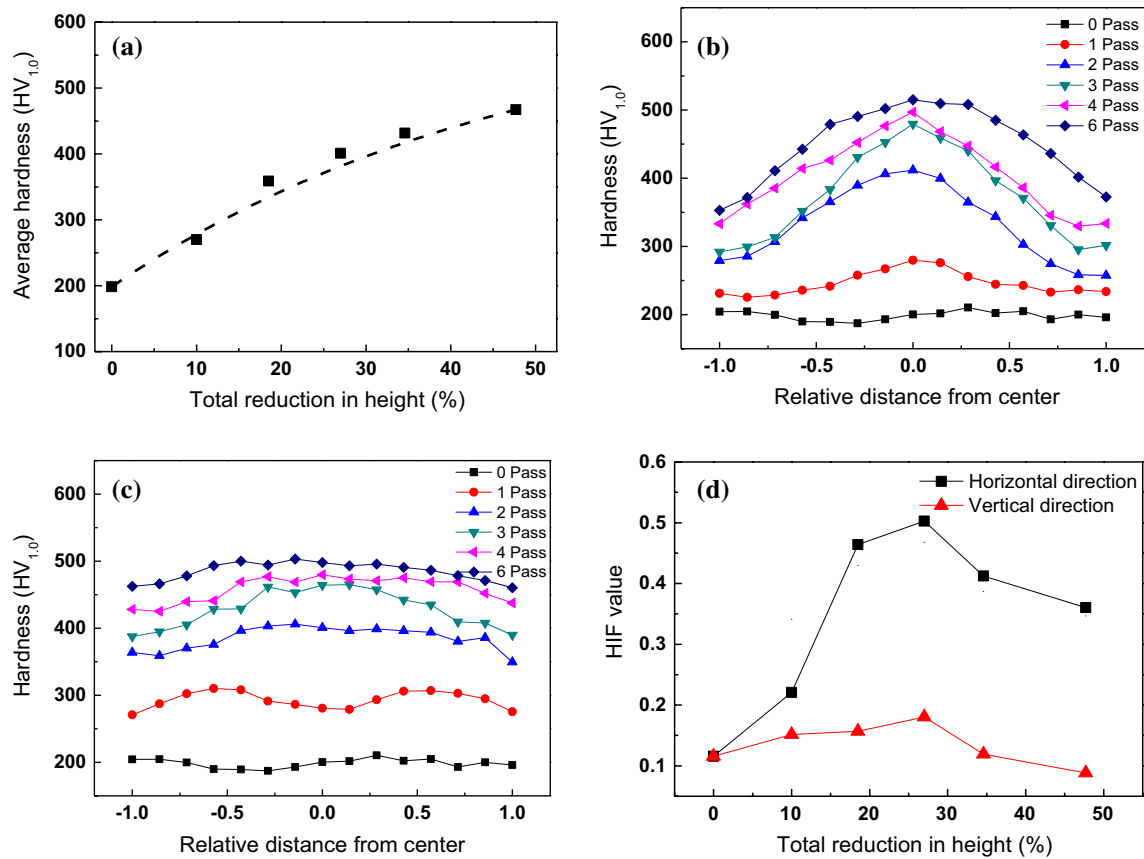


Fig. 3 Comparison of measured **a** average hardness, **b** hardness profiles along the horizontal direction, **c** hardness profiles along the vertical direction, and **d** hardness inhomogeneity factor (HIF) with total reduction in height of rolled wire

3.2 Analysis of Strain and Stress

According to the results of hardness test, the wire processed by flat rolling process had an inhomogeneous deformation with area. Although flat rolling process with round wire looks simple, the workpiece experiences complex three-dimensional deformation stemming from the initial shape of round wire, indicating that analytic approach on the stress and strain distribution of flat rolled wire is impossible. Accordingly, FE analysis is strongly necessary to have detailed information on the strain and stress distribution of flat rolled wire. Commercial DEFORM FE software was utilized for simulating the flat rolling process of wire with three-dimensional module. For numerical simulation, the necessary stress–strain curves for input data are obtained by fitting the tensile or compressive stress–strain curves. Typically, the influences of strain rate and temperature can be ignored during cold forming process and therefore Hollomon's type stress–strain curves are inserted. However, it is well known that TWIP steels show both positive strain rate sensitivity (PSRS) and negative strain rate sensitivity (NSRS) with strain rate and chemical composition. Similar to FCC metals, the TWIP steels without C content tend to

show PSRS [42], which means the tensile strength increases with strain rate. In contrast, C-bearing TWIP steels showed both NSRS and PSRS with strain rate, and critical strain rate for transition from NSRS to PSRS was changed with chemical compositions, which was generally explained by different DSA effect with strain rate and chemical composition. That is, the C-bearing TWIP steels showed NSRS in the lower region of strain rate [43–45] and PSRS in the higher region of strain rate [46]. Note that NSRS was also observed at the higher strain rate region in some C-bearing TWIP steels [47]. In case of similar alloying system in the strain rate range of 10^{-3} – 10^0 s⁻¹, most of the TWIP steels showed NSRS with strain rate. For instance, Yang et al. [48] reported that the Fe–22Mn–0.6C–1.5Al TWIP steel had the strain rate sensitivity value (m) of -0.014 in the strain rate range of 10^{-4} – 10^0 s⁻¹. It should be noted that the average strain rate is between 0.69 and 0.92 s⁻¹ during flat rolling process in this study (Table 2). The fitted tensile curve at the strain rate of 10^{-3} (Fig. 2b) using Hollomon's law can be described as following equation:

$$\sigma = 1884\epsilon^{0.43} \quad (4)$$

For more reliable results of numerical simulation, the effect of strain rate was considered in the input stress–strain curve for numerical simulation, which is represented as follows:

$$\sigma = 1884\epsilon^{0.43} \left(\frac{\dot{\epsilon}}{10^{-3}} \right)^{-0.014} \quad (5)$$

The wire was assumed to be isotropic since hot rolled wire was used as an initial material in this experiment. And it is still necessary to consider the kinematic hardening behavior of TWIP steel in order to improve the prediction accuracy of deformed wire due to the strong kinematic hardening behavior of TWIP steels [49]. However, the kinematic hardening behavior of TWIP steels was not considered in this simulation stemming from the small strain path changes during flat rolling process.

All of the rolls were considered as a rigid body and the initial wire of 13 mm in diameter was rolled with an average reduction in height per pass of 10%. The friction factor of 0.3 was selected [4] and the other process parameters were kept the same as the experimental conditions as shown in Table 2. The effect of temperature rise during process was neglected due to the low rolling speed of 5 RPM and relatively small reduction in height per pass of 10%. The quarter of full geometry was simulated stemming from the

symmetrical nature of flat rolling process in order to reduce the computational cost. Brick type mesh with 300 elements in cross section of wire was used and finer meshes were employed in surface area to improve the accuracy of results. Figure 4 shows the distribution of effective strain in the cross section of rolled wire from first pass to final pass.

The distribution of effective strain in flat rolled wire was very complex with area. The center area tended to have a peak effective strain and free surface area tended to have a lower effective strain value at all the passes. During the first and second passes, the center area did not have the maximum strain since external force generated from the roll contact area did not penetrate into center area, which is consistent with the result of measured hardness profiles along the vertical direction (Fig. 3c). That is, the strain was localized in the vicinity of wire-roll contact area at small reduction in height. After the third pass, center area had the maximum effective strain, and the trend of effective strain distribution was similar to the wires of the fourth, fifth, and sixth passes. It is interesting to note that the strain distribution depended on the material properties such as strain hardening exponent (n) value or strain hardening rate. According to the result of Kazeminezhad and Karimi Taheri [25], Cu wire had the maximum strain at center area at the reduction in height of 14%, which is totally different with the present results of

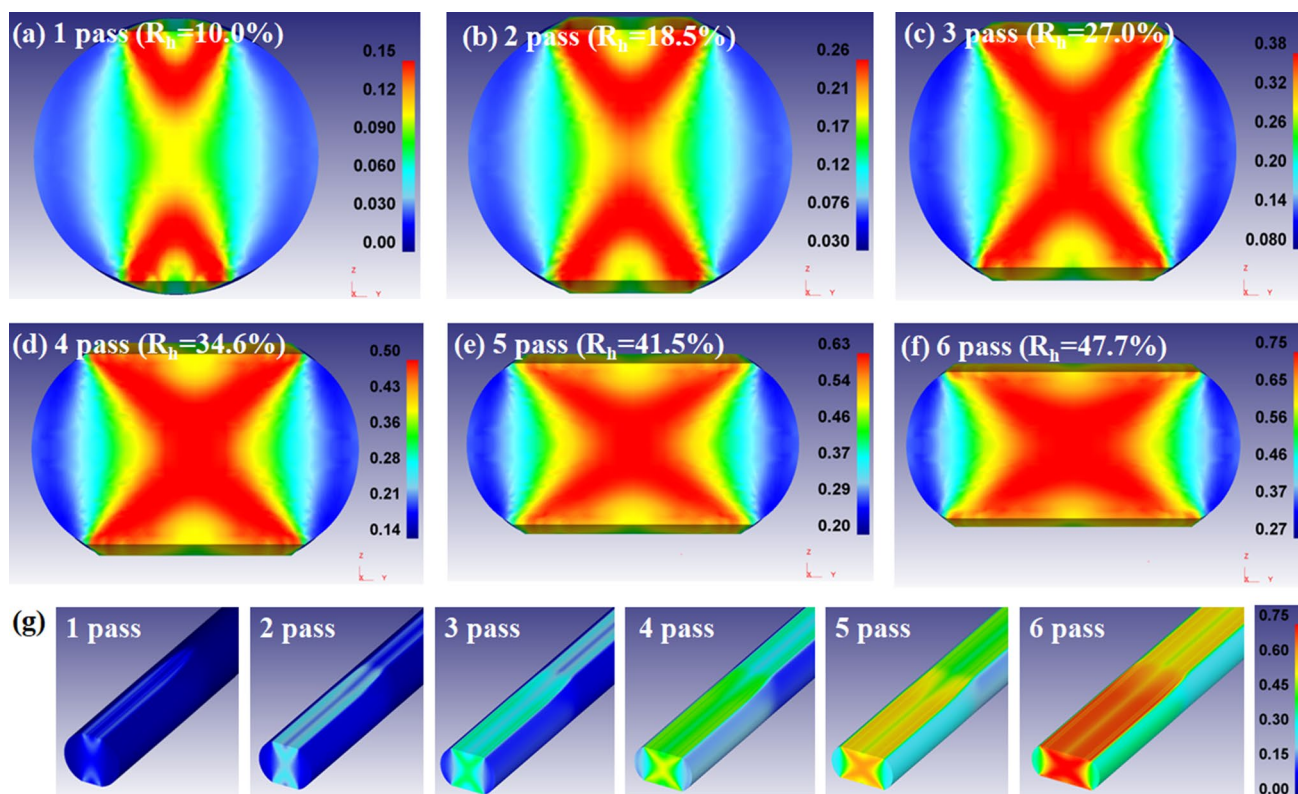


Fig. 4 Contour maps of effective strain of flat rolled wires **a–f** with different scale and **g** with same scale as a function of total reduction in height

effective strain (Fig. 4a, b) and measured hardness (Fig. 3c). Based on the author’s experiences, this different deformation behavior with materials is highly related to the n value of materials. Two macroscopic shear bands with high effective strain were clearly observed in the cross section of flat rolled wires due to the deformation inhomogeneity. This shape of macroscopic shear bands was well reported in several compression type metal forming processes such as compression process [50], side pressing process [51], caliber rolling process [1], flat roll drawing process [3], and flat rolling of wire process [24]. This is due to the less deformation or restricted plastic flow in the region around the interface between workpiece and tools under the compressive stress. The region of shear bands was harder than the other regions due to the higher strain, which means the shear band leads to the inhomogeneity of mechanical properties with area of flat rolled wire. It is expected that the deviation of mechanical properties with area of flat rolled TWIP steel wire was higher in

comparison with the plain carbon steels and Cu wires due to the higher strain hardening rate of TWIP steels [39].

The effective strain along the horizontal and vertical directions was extracted from the contour maps by FE analysis as shown in Fig. 5. The maximum effective strain occurred around quarter area after first pass and center area after third pass. The free surface area always had the minimum effective strain during the whole rolling process. The difference of effective strain along the horizontal direction was much higher than that of the vertical direction, which is consistent with the result of Vickers hardness test. The similar result was also reported in flat rolled Cu wire [25]. Clearly, the maximum difference of effective strain and/or hardness occurred in between center area and free surface area of flat rolled wire.

Figure 6 depicts the schematic of stress state and strain level at each area of flat rolled wire based on the FE analysis. The length of red arrow means the stress magnitude for each direction. All the areas were elongated along the rolling direction and compressed along the vertical direction. The center area had higher vertical stress originating from the stress penetration from roll contact surface and symmetrical condition of specimen during flat rolling process. The free surface area had relatively low compressive stress and this area was easily elongated along the horizontal direction due to the no restriction of plastic flow. The stress state of roll contact area was similar to plane strain condition such as cold rolling of plate although detailed investigation [17, 52, 53] showed that the distribution of contact pressure at roll contact area is complex along the rolling and width directions of wire.

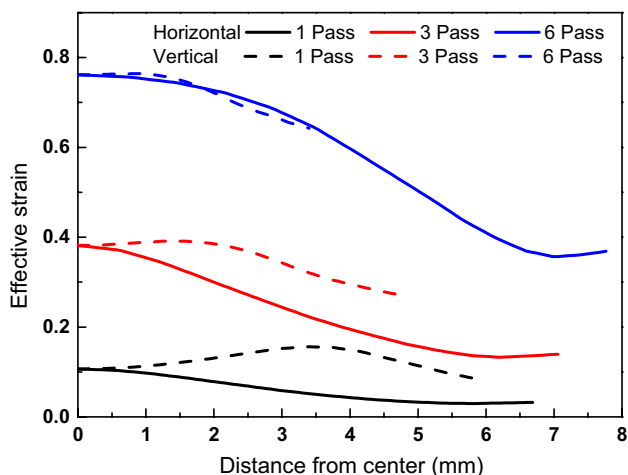
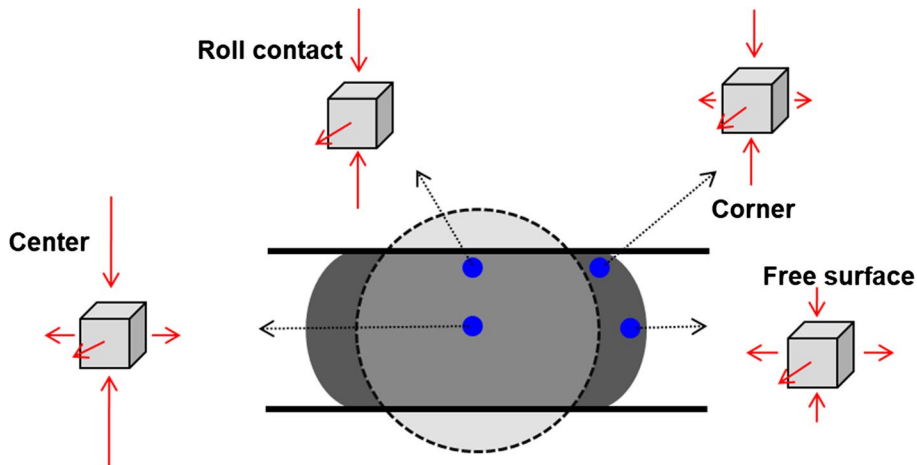


Fig. 5 Comparison of effective strain along the radial direction with reduction in height based on the numerical simulation

3.3 Evolution of Microstructure

The microstructure of hot rolled steel consists of fully recrystallized grains with an average grain size of 12 μm and a weak texture as shown in Fig. 7. Annealing twins can be

Fig. 6 Schematic of stress state and strain level at each area in flat rolled wire



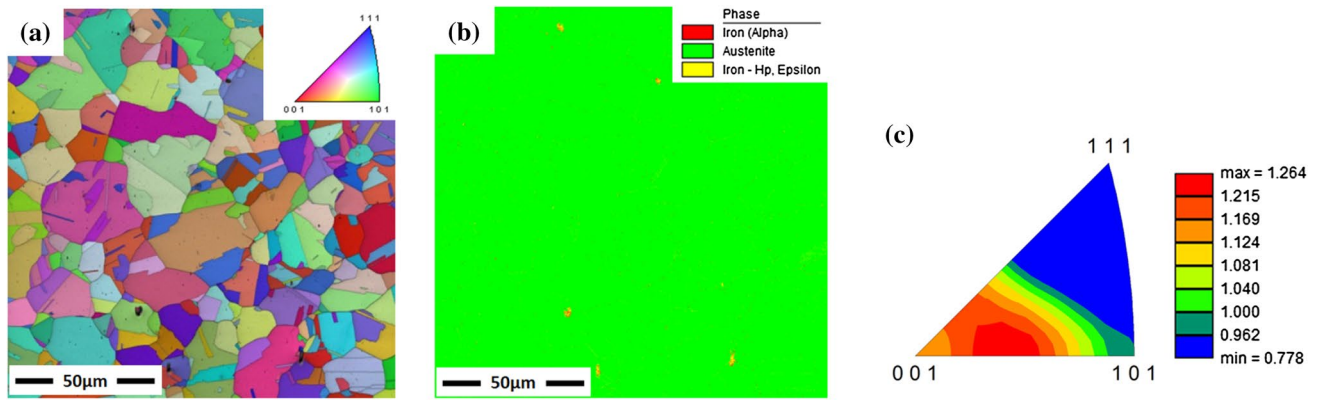


Fig. 7 EBSD **a** IPF map, **b** phase map, and **c** texture of hot rolled steel

seen but no deformation twin was observed. Figure 7b shows the result of phase map for the hot rolled steel, indicating a high mechanical stability of austenite phase because no other phase was detected. In addition, no other phase except austenite was observed during flat rolling process due to the SFE of 27.2 mJ/m² in the present material.

To understand the microstructure and texture during flat rolling process of wire, rolled specimens were analyzed by EBSD. Figure 8 shows the image quality (IQ), inverse pole figure (IPF), and Kernel average misorientation (KAM) maps at the reduction in height of 10% in the four individual sites, i.e., center, free surface, roll contact surface, and corner. The EBSD maps were measured at cross section plane perpendicular to the rolling direction. Parallel black lines inside grain in IQ maps were twin bundles consisting of several thin deformation twins [28, 54]. Several grains had deformation twins at center and corner areas despite the lower reduction in height of 10% as shown in Fig. 8a, d; whereas, a few deformation twins were observed at free surface and roll contact areas as shown in Fig. 8b, c, whose behavior was highly related to the distribution of effective strain with areas (Fig. 4a). Especially, no deformation twin was observed at free surface area since free surface area had lower strain than any other areas during flat rolling process. Meanwhile, at the height reduction of 10%, the twin density of center area was lower than that of corner area since center area had a lower effective strain compared to corner area (Fig. 4a).

Comparing Fig. 8, twin volume fraction of flat rolled wire was increased regardless of areas at the height reduction of 27% as shown in Fig. 9. Most of the grains had deformation twin at center area (Fig. 9a) and the twin density of center area was higher than any other areas due to the highest effective strain as shown in Fig. 4c. On the other hand, the density of twin at free surface area was lowest due to the lower strain level. Corner area had a relatively high twin density since macroscopic shear band

occurred from center to corner area as shown in Fig. 4. From the Fig. 9e, it is evident that grains in center area were elongated along the horizontal direction stemming from the higher compressive stress as shown in Fig. 6. Meanwhile, no shape change of grain was found in the corner, roll contact, and free surface areas. In view of grain orientation, no strong texture was observed in all the areas as shown in Figs. 8 and 9.

It is generally accepted that the local orientation difference has a relationship with the magnitude of plastic deformation [55], thus misorientation mapping is widely used to evaluate the amount of plastic deformation in the field of mechanical engineering. Figure 10 compared KAM value as a function of total reduction in height with area based on the EBSD KAM maps. KAM value was calculated with the maximum misorientation angle of 5° within the third neighboring shell. Comparing Figs. 8 and 9, KAM became stronger as the specimen experienced higher reduction in height. Center and corner areas had higher KAM distribution compared to free surface and roll contact areas. Especially, the free surface area had the lowest KAM distribution, which is consistent with the result of distribution of deformation twin (Figs. 8 and 9), effective strain (Fig. 4), and hardness (Fig. 3).

It is evident from the analysis of the deformation twin and KAM value that center area of flat rolled wire tends to have the highest twin density and KAM value. This higher twin formation increased the activation of so-called dynamic Hall–Petch effect in TWIP steel and higher KAM value meant higher geometrically necessary dislocation (GND) density, resulting in higher strength during plastic deformation. Whereas, free surface area showed the lowest twin density and KAM value during the whole rolling process, leading to the relatively low dynamic Hall–Petch hardening and GND hardening, resulting in low strength. This explanation is in good agreement with the results of hardness test in Fig. 3.

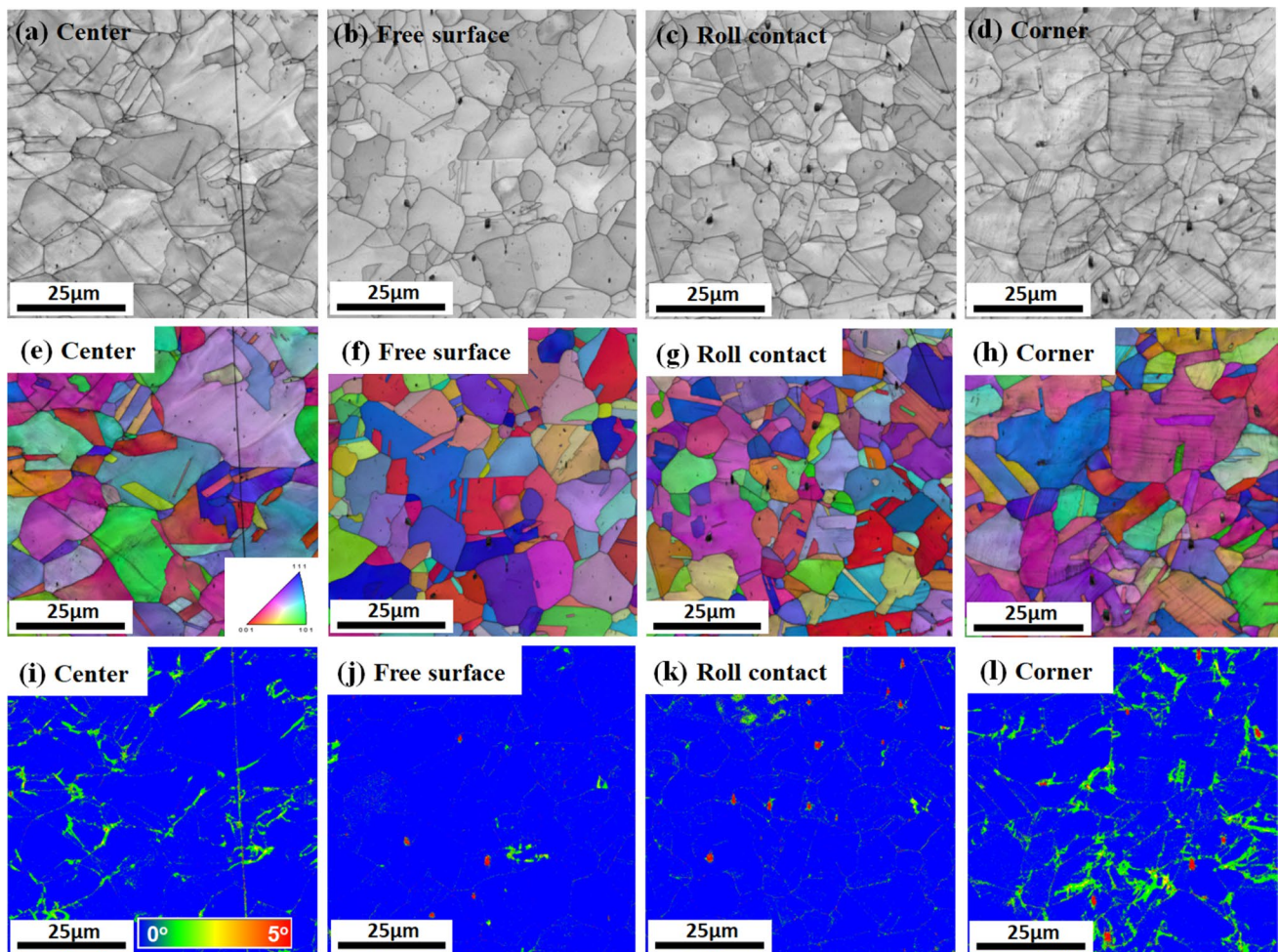


Fig. 8 Comparison of a–d IQ, e–h IPF, and i–l KAM maps with area at the reduction in height of 10%

3.4 Shape Change of Rolled Wire

During flat rolling process, the variation of lateral spread (W) and width of contact area (b) with reduction in height should be known and understood since undesirable shape of rolled wire leads to unsatisfactory products. Especially, it is necessary to estimate the W value with external process conditions and materials because we cannot directly control the amount of lateral spread of flat rolled wire due to the free surface of round shape wire. Table 3 summarizes the measured cross-sectional shape of flat rolled wires in each pass and Fig. 11 shows the variations of experimental and numerically simulated W and b values of TWIP steel with total reduction in height. It is clearly observed that the W and b values increased with reduction in height. The W and b values analyzed by numerical simulation were in good agreement with the results of measured data. However, they had small deviations, especially the magnitude of deviation slightly increased with increasing total reduction in height. The maximum discrepancy between experimental values

and numerically simulated values was 4.9% for W value and 5.9% for b value. Based on the author's experiences and literature review, this discrepancy was highly related to the friction coefficient of wire-roll interface, material anisotropy, and applied hardening model. In this study, the friction coefficient of 0.3 was assumed and the workpiece was assumed to be isotropic. Masse et al. [21] increased the prediction accuracy of W value in pearlitic steel wire during flat rolling process by taking into account anisotropy of material: discrepancy was improved from 10 to 5% underestimations using anisotropic model. Especially, the anisotropic model is strongly necessary to evaluate the deformation behaviors of free surface in material during cold forming process. A well-defined kinematic hardening model is also necessary to improve the prediction accuracy of deformed material [56].

To understand the effect of material properties on the W value of flat rolled wire, the W value in TWIP steel was compared with plain carbon steels in the literature by Kazeminezhad and Karimi Taheri [19] as shown in Fig. 12. They proposed the following relationship between lateral

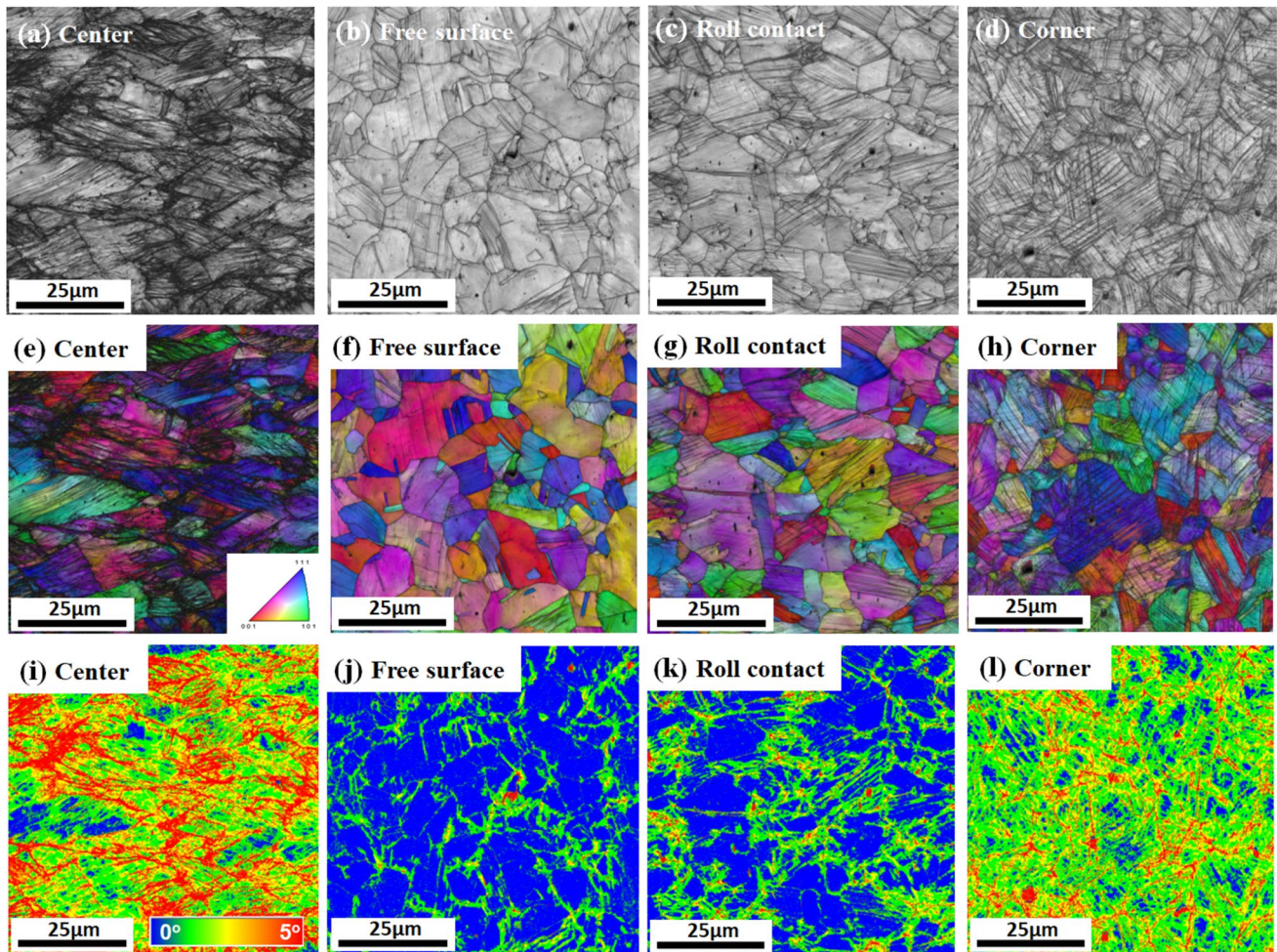


Fig. 9 Comparison of **a–d** IQ, **e–h** IPF, and **i–l** KAM maps with area at the reduction in height of 27%

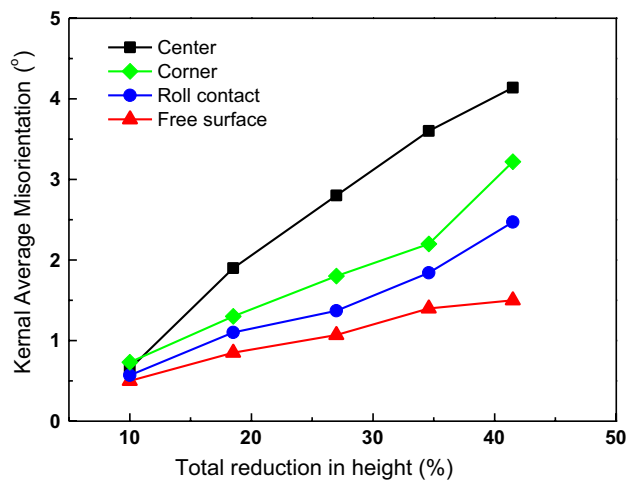


Fig. 10 Variations in average KAM as a function of total reduction in height and area

spread and reduction in height of low and high carbon steels using the spread formula of Wusatowski [57].

$$\frac{W_1}{W_0} = 1.02 \left(\frac{h_0}{h_1} \right)^{0.45} \quad (6)$$

In this study, the lateral spread of TWIP steel with reduction in height was lower than that of plain carbon steels, and had a following relationship:

$$\frac{W_1}{W_0} = 0.996 \left(\frac{h_0}{h_1} \right)^{0.404} \quad (7)$$

The above type of equation adopted by Kazeminezhad and Karimi Taheri [19] estimated the variations in lateral spread of flat rolled TWIP steel wire with high degree of accuracy in all the range of reduction in height since the R-squared value for the curve fitting using Eq. (7) was higher than 0.99 as shown in Fig. 12. Meanwhile, the coefficients of parameter were different with materials, indicating that

Table 3 Measured cross section of flat rolled TWIP steel wires in this experiment

No. of pass	Roll gap (mm)	Measured wire size (mm)			Total reduction in height (%)
		Height (h)	Width (W)	Width of contact area (b)	
–	–	13.0	13.0	–	–
1	11.63	11.7	13.4	4.8	10.0
2	10.50	10.6	14.1	6.8	18.5
3	9.40	9.5	14.8	8.5	27.0
4	8.45	8.5	15.4	9.9	34.6
5	7.50	7.6	16.2	11.3	41.5
6	6.75	6.8	16.7	12.7	47.7

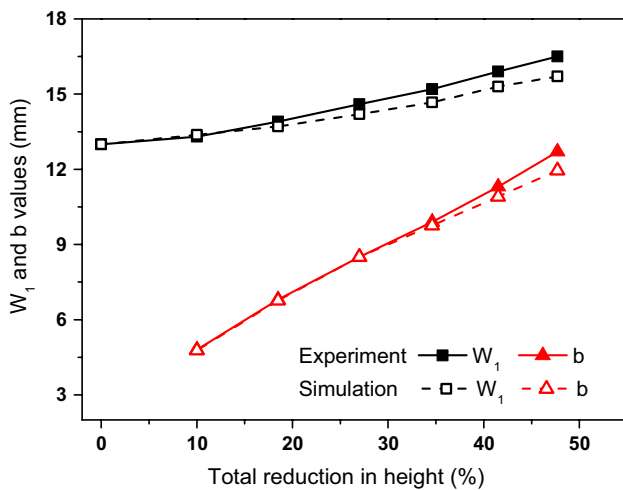


Fig. 11 Comparison of measured and numerically simulated W and b values with total reduction in height of TWIP steel

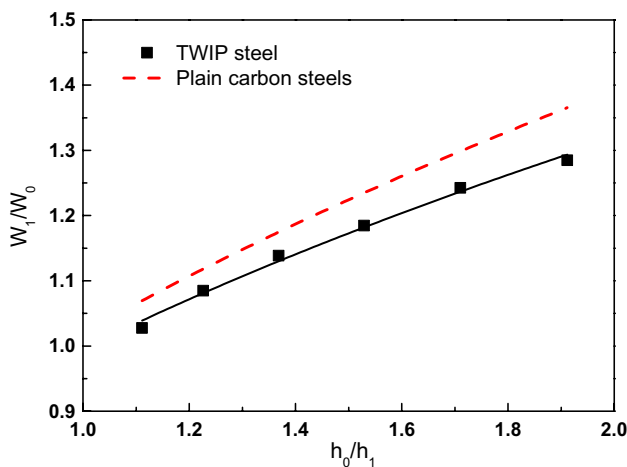


Fig. 12 Comparison of relationship between W_1/W_0 and h_1/h_0 in TWIP steel and plain carbon steels [19]

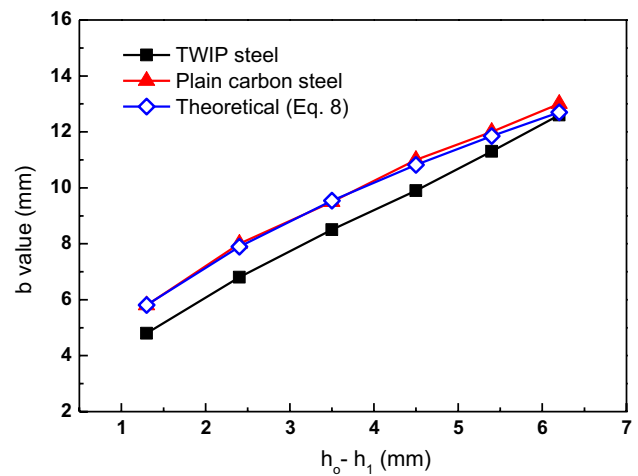


Fig. 13 Comparison of b value with reduction in height between TWIP steel and plain carbon steels [18]

the lateral spread of flat rolled wire was different with materials. That is, TWIP steel was less spread compared to the plain carbon steels. This different behavior between TWIP steel and plain carbon steels might be related to the different experimental conditions such as roll diameter, way of reduction in height, friction condition [22], and rolling speed [18]. However, to the best of author’s knowledge, it is highly related to the strain hardening behavior of material. The n value of Hollomon’s law in TWIP steel is a range from 0.4 to 0.6, whereas n value of plain carbon steels is from 0.1 to 0.3. For instance, Eom et al. [50] reported that SCM435 steel with high strain hardening rate had a lower lateral spread compared to PHTS steel with low strain hardening rate during upsetting test.

Another critical parameter in flat rolling process of wire is the width of contact area of wire. For the comparative study, the b values from plain carbon steel reported by Kazeminezhad and Karimi Taheri [18] are also given in Fig. 13. The b value strongly depended on reduction in height of wire: the b value increased with increasing reduction in height of wire. Interestingly, the b value of TWIP steel is lower than

that of plain carbon steel and theoretical relation suggested by Kazeminezhad and Karimi Taheri [18] as follows:

$$b = \sqrt{2\Delta h h_0} \tag{8}$$

The difference of W value of flat rolled wire with materials (Fig. 12) might be related to the difference of b value with materials, and the behaviors of W and b values depended on the n value of material. For better understanding of the effect of material properties on shape change in flat rolled wire, the dependence of strain hardening coefficient (K) and n value of Hollomon’s law on shape change of wire was evaluated using numerical simulation since the W and b values

predicted by numerical simulation were in good agreement with the measured values as shown in Fig. 11. For the systematic study considering TWIP steel in this study and low strength materials, K and n values were varied in the range of 50–1884 MPa and 0.01–0.43, respectively. The strain rate effect was not considered in this simulation.

Figure 14 shows the distribution of effective strain in the cross section of flat rolled wire at the reduction in height of 27% with different K and n values. Interestingly, it was found that the distribution of effective strain with area was quite different with n value. The larger inhomogeneity of effective strain with area was observed in

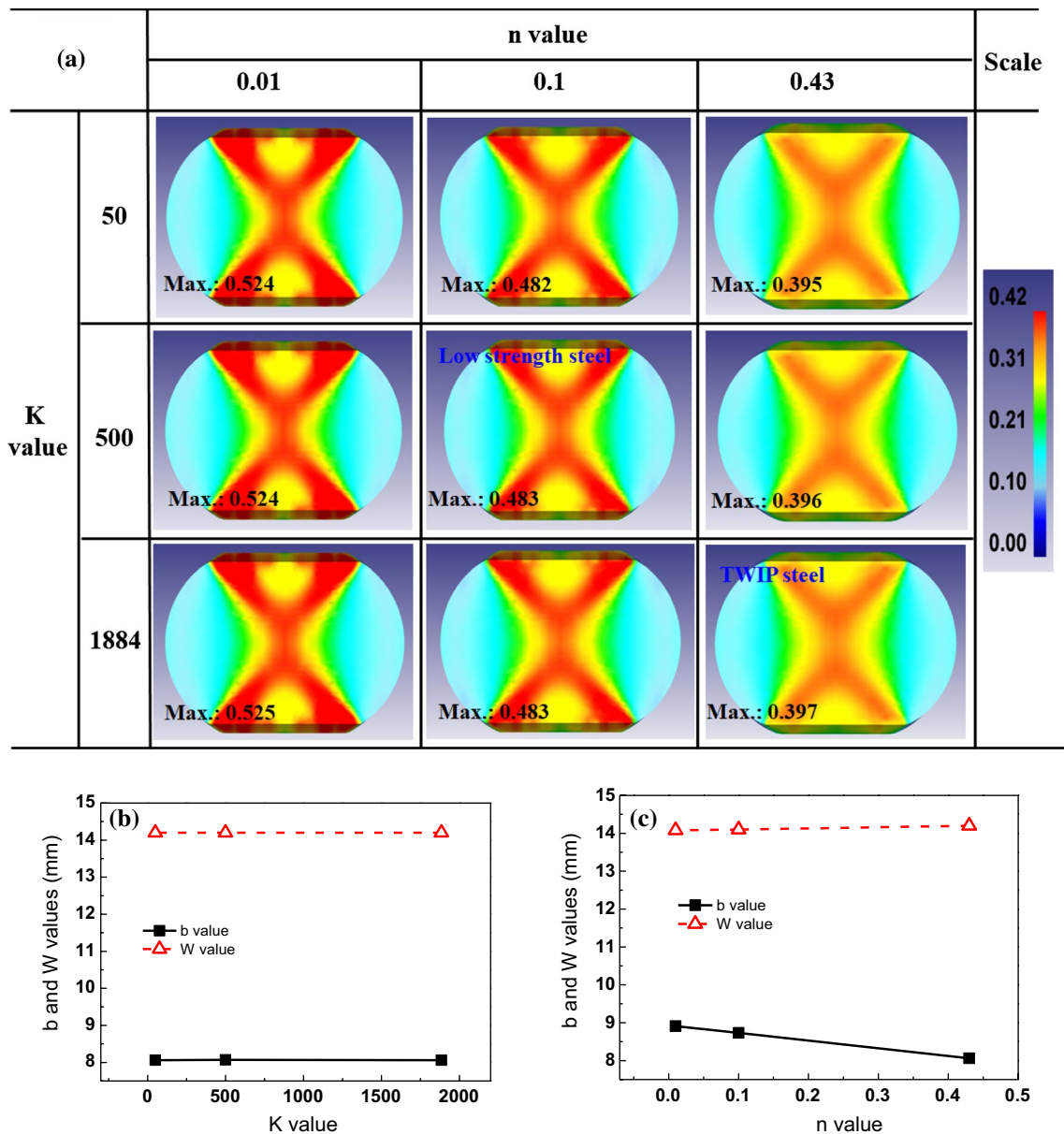


Fig. 14 a Contour maps of effective strain with different K and n values, and variation of W and b values with b K value and c n value at the reduction in height of 27%

materials having lower n value. Accordingly, the stronger shear band was seen in the low hardening material compared to the high hardening material. For instance, TWIP steels had a lower inhomogeneity of effective strain with area compared to plain carbon steels or Cu wires. Meanwhile, the strain distribution of rolled wire was independent of K value since the distribution of effective strain was similar regardless of K value. To evaluate b and W values of rolled wire with K and n values quantitatively, b and W values are represented with K value (Fig. 14b) and n value (Fig. 14c). Apparently, the b and W values were constant with K value. Meanwhile, the b value was decreased with increasing n value, which is consistent with the experimental results: TWIP steels with higher n value had lower b value compared to plain carbon steels with lower n value as shown in Fig. 13. This is due to the easier metal flow of low hardening materials along the dies or tools during plastic forming process. Similar phenomena were reported in equal channel angular pressing [58] and bolting [50] processes. More interestingly, the W value was almost constant with n value, which is an unexpected result. Experimental comparison between TWIP steel and plain carbon steels (Fig. 12) revealed that plain carbon steels with low strain hardening rate had higher W values than TWIP steel. This discrepancy between experimental result and numerically simulated result was related to the assumptions of numerical simulation in this study. It is reported that W value depends on the friction coefficient of wire-roll interface [22] and material anisotropy [21] during flat rolling process. In this study, the friction coefficient of 0.3 was assumed and the workpiece was assumed to be isotropic. To increase the prediction accuracy of the shape at free surface area in material during forming process, the anisotropic model including kinematic hardening as well as proper process parameter values was strongly necessary. Also, it should be noted that the plain carbon steels in the literatures of [18, 19] were flat-rolled in single pass using different rolling reductions, whereas TWIP steel in this study was rolled using multiple pass rolling. This could be one of the reasons that TWIP steel had lower W value than plain carbon steels, but the effect was not large since TWIP steel had lower W value than plain carbon steels from the first pass, which is the same process condition to the plain carbon steels in the literatures. Nevertheless, further research might be necessary to find a direct relationship between n value and W value of flat rolled wire.

Overall, based on the experimental and numerical results achieved in this comparison study with plain carbon steels, it is concluded that material properties such as n value strongly affected the shape of flat rolled wire. That is, material properties are crucial parameters that influence the deformation behavior of flat rolled wire. Consequently, to make flat rolled

wire products with desired shape, we need to consider the material properties as well as external process conditions during flat rolling process of wire.

4 Conclusions

The mechanical properties, effective strain, microstructure, and shape change of TWIP steel wire were systematically studied during flat rolling process, and then the results were compared with plain carbon steels. The following major conclusions were thus arrived from the results:

1. A very different behavior of hardness, strain, twinning, and KAM value was observed with areas of flat rolled wire since specimen had different stress state and strain with areas during flat rolling process. The center area tends to have the maximum twin density, KAM value, effective strain, and hardness; whereas free surface area had the minimum values.
2. The HIF values along the horizontal direction were much higher in comparison with those of the vertical direction. For instance, the maximum HIF value along the horizontal direction was about three times higher than that along the vertical direction. HIF value gradually increased and then decreased with reduction in height, which means the maximum HIF value occurred at the specific reduction in height, i.e., 27%. This result is greatly useful in industrial applications since one can produce flat rolled wires with more homogeneous mechanical properties by controlling the total reduction in height of wire.
3. The W and b values of flat rolled TWIP steel wire were lower than those of plain carbon steels. It means that material properties such as strain hardening exponent are crucial parameters that influence the deformation behavior of flat rolled wire; therefore, we need to consider the material properties as well as external process conditions during flat rolling process of wire to make flat rolled wire products with proper and desired shape.

Acknowledgements This Research was supported by National Research Foundation of Korea (NRF-2018R1D1A1B07050103) and the Tongmyong University Research Grants 2019 (2019F005).

References

1. J.K. Hwang, *Mater. Sci. Eng. A* **711**, 156 (2018)
2. R. Iankov, *J. Mater. Process. Technol.* **142**, 355 (2003)
3. F. Lambiase, A.D. Ilio, *J. Manuf. Process.* **14**, 208 (2012)
4. T. Inoue, F. Yin, Y. Kimura, *Mater. Sci. Eng. A* **466**, 114 (2007)

5. F. Yin, T. Hanamura, T. Inoue, K. Nagai, *Metall. Mater. Trans. A* **35A**, 665 (2004)
6. T. Inoue, F. Yin, Y. Kimura, K. Tsuzaki, S. Ochiai, *Metall. Mater. Trans. A* **41A**, 341 (2010)
7. S. Torizuka, E. Muramatsu, S.V.S.N. Murty, K. Nagai, *Scr. Mater.* **55**, 751 (2006)
8. Y.S. Oh, I.H. Son, K.H. Jung, D.K. Kim, D.L. Lee, Y.T. Im, *Mater. Sci. Eng. A* **528**, 5833 (2011)
9. T. Lee, C.H. Park, S.Y. Lee, I.H. Son, D.L. Lee, C.S. Lee, *Met. Mater. Int.* **18**, 391 (2012)
10. Y.S. Chun, J. Lee, C.M. Bae, K.T. Prak, C.S. Lee, *Scr. Mater.* **67**, 681 (2012)
11. T. Lee, M. Koyama, K. Tsuzaki, Y.H. Lee, C.S. Lee, *Mater. Lett.* **75**, 169 (2012)
12. T. Mukai, H. Somekawa, T. Inoue, A. Singh, *Scr. Mater.* **62**, 113 (2010)
13. T. Lee, K.T. Park, D.J. Lee, J. Jeong, S.H. Oh, H.S. Kim, C.H. Park, C.S. Lee, *Mater. Sci. Eng. A* **648**, 359 (2015)
14. G. Krallics, J. Gubicza, Z. Bezi, I. Barkai, *J. Mater. Process. Technol.* **214**, 1307 (2014)
15. J. Lee, J. Park, H. Jeong, *Mater. Lett.* **222**, 122 (2018)
16. J.G. Kim, M.I. Latypov, D.J. Lee, H.G. Jeong, J.B. Lee, S. Lee, H.S. Kim, *Metall. Mater. Trans. A* **46**, 260 (2014)
17. C. Vallellano, P.A. Cabanillas, F.J. Garcia-Lomas, *J. Mater. Process. Technol.* **195**, 63 (2008)
18. M. Kazeminezhad, A. Karimi Taheri, *Mater. Des.* **26**, 99 (2005)
19. M. Kazeminezhad, A. Karimi Taheri, *J. Mater. Process. Technol.* **160**, 313 (2005)
20. M. Kazeminezhad, A. Karimi Taheri, A.K. Tieu, *J. Mater. Process. Technol.* **200**, 325 (2008)
21. T. Masse, Y. Chastel, P. Montmitonnet, C. Bobadilla, N. Persem, S. Foissey, *J. Mater. Process. Technol.* **211**, 103 (2011)
22. H. Utsunomiya, P. Hartley, I. Pillinger, *J. Manuf. Sci. Eng.* **123**, 397 (2001)
23. A. Parvizi, B. Pasoodeh, K. Abrinia, H. Akbari, *J. Mater. Process. Technol.* **20**, 245 (2015)
24. M. Kazeminezhad, A. Karimi Taheri, *Mater. Lett.* **60**, 3265 (2006)
25. M. Kazeminezhad, A. Karimi Taheri, *Mater. Des.* **28**, 2047 (2007)
26. M. Kazeminezhad, A. Karimi Taheri, *J. Mater. Process. Technol.* **202**, 553 (2008)
27. T. Masse, Y. Chastel, P. Montmitonnet, C. Bobadilla, N. Persem, S. Foissey, *Int. J. Mater. Form.* **5**, 129 (2012)
28. J.K. Hwang, I.C. Yi, I.H. Son, J.Y. Yoo, B. Kim, A. Zargaran, N.J. Kim, *Mater. Sci. Eng. A* **644**, 41 (2015)
29. J.K. Hwang, I.H. Son, J.Y. Yoo, A. Zargaran, N.J. Kim, *Met. Mater. Int.* **21**, 815 (2015)
30. O. Bouaziz, S. Allain, C.P. Scott, P. Cugy, D. Barbier, *Curr. Opin. Solid State Mater. Sci.* **15**, 141 (2011)
31. O. Grassel, L. Kruger, G. Frommeyer, L.W. Meyer, *Int. J. Plast.* **16**, 1391 (2000)
32. D. Barbier, N. Gey, S. Allain, N. Bozzolo, M. Humbert, *Mater. Sci. Eng. A* **500**, 196 (2009)
33. J.E. Jin, Y.K. Lee, *Mater. Sci. Eng. A* **527**, 157 (2009)
34. H. Idrissi, K. Renard, D. Schryvers, P.J. Jacques, *Scr. Mater.* **63**, 961 (2010)
35. O.A. Zambrano, *J. Mater. Sci.* **53**, 14003 (2018)
36. J.E. Jung, J. Park, J. Kim, J.B. Jeon, S.K. Kim, Y.W. Chang, *Met. Mater. Int.* **20**, 27 (2014)
37. Z.C. Luo, M.X. Huang, *Scr. Mater.* **142**, 28 (2018)
38. K.H. So, J.S. Kim, Y.S. Chun, K.T. Park, Y.K. Lee, C.S. Lee, *ISIJ Int.* **49**, 1952 (2009)
39. J.K. Hwang, *J. Mater. Sci.* **54**, 8743 (2019)
40. A. Saeed-Akbari, J. Imlau, U. Prahla, W. Bleck, *Metall. Mater. Trans. A* **40**, 3076 (2009)
41. J.E. Jin, Y.K. Lee, *Acta Mater.* **60**, 1680 (2012)
42. J.T. Benzinger, W.A. Poling, D.T. Pierce, J. Bentley, K.O. Findley, D. Raabe, J.E. Wittig, *Mater. Sci. Eng. A* **711**, 78 (2018)
43. H.K. Yang, Z.J. Zhang, Y.Z. Tian, Z.F. Zhang, *Mater. Sci. Eng. A* **690**, 146 (2017)
44. S.Y. Lee, S.I. Lee, B. Hwang, *Mater. Sci. Eng. A* **711**, 22 (2018)
45. H.K. Yang, Z.J. Zhang, Z.F. Zhang, *Mater. Sci. Eng. A* **622**, 184 (2015)
46. A.S. Hamada, A. Kisko, A. Khosravifard, M.A. Hassan, L.P. Karjalainen, D. Porter, *Mater. Sci. Eng. A* **712**, 255 (2018)
47. Z.Y. Liang, X. Wang, W. Huang, M.X. Huang, *Acta Mater.* **88**, 170 (2015)
48. H.K. Yang, Z.J. Zhang, F.Y. Dong, Q.Q. Duan, Z.F. Zhang, *Mater. Sci. Eng. A* **607**, 551 (2014)
49. G. Joo, H. Huh, *Int. J. Mech. Sci.* **146–147**, 432 (2018)
50. J.G. Eom, Y.H. Son, S.W. Jeong, S.T. Ahn, S.M. Jang, D.J. Yoon, M.S. Joun, *Mater. Des.* **54**, 1010 (2014)
51. S.L. Semiatin, J.J. Jonas, *Formability and Workability of Metals: Plastic Instability and Flow Localization*, vol. 71 (American Society for Metals, USA, 1984)
52. B. Carlsson, *J. Mater. Process. Technol.* **73**, 1 (1998)
53. M. Kazeminezhad, A. Karimi Taheri, *J. Mater. Process. Technol.* **171**, 253 (2006)
54. K. Jeong, J.E. Jin, Y.S. Jung, S. Kang, Y.K. Lee, *Acta Mater.* **61**, 3399 (2013)
55. A.J. Schwartz, M. Kumar, B.L. Adams, D.P. Field, *Electron Backscatter Diffraction in Materials Science*, 2nd edn. (Springer, 2009) pp. 251–262
56. B.W. Williams, C.H.M. Simha, N. Abedrabbo, R. Mayer, M.J. Worswick, *Int. J. Impact Eng.* **37**, 652 (2010)
57. Z. Wusatowski, *Fundamentals of Rolling* (Pergamon Press, London, 1969), pp. 87–107
58. H.S. Kim, M.H. Seo, S.I. Hong, *Mater. Sci. Eng. A* **291**, 86 (2000)

Publisher's Note Springer Nature remains neutral with regard to jurisdictional claims in published maps and institutional affiliations.